

HOW PRECISELY COULD WE IDENTIFY WIMPS MODEL-INDEPENDENTLY WITH DIRECT DARK MATTER DETECTION EXPERIMENTS

MANUEL DREES

*Physikalisches Institut and Bethe Center of Theoretical Physics
Universität Bonn, D-53115 Bonn, Germany
E-mail: drees@th.physik.uni-bonn.de*

CHUNG-LIN SHAN*

*School of Physics and Astronomy, Seoul Nat'l Univ., Seoul 151-747, Republic of Korea
E-mail: cshan@hep1.snu.ac.kr*

In this talk we present data analysis methods for reconstructing the mass and couplings of Weakly Interacting Massive Particles (WIMPs) by using directly future experimental data (i.e., measured recoil energies) from direct Dark Matter detection. These methods are independent of the model of Galactic halo as well as of WIMPs. The basic ideas of these methods and the feasibility and uncertainties of applying them to direct detection experiments with the next generation detectors will be discussed.

Keywords: Dark Matter; WIMP; direct detection; direct detection simulation

1. Introduction

Weakly Interacting Massive Particles (WIMPs) χ arising in several extensions of the Standard Model of electroweak interactions with masses roughly between 10 GeV and a few TeV are one of the leading candidates for Dark Matter^{1, 2}. Currently, the most promising method to detect different WIMP candidates is the direct detection of the recoil energy deposited by elastic scattering of ambient WIMPs on the target nuclei^{3, 4}. The differential event rate for elastic WIMP–nucleus scattering is given by¹:

$$\frac{dR}{dQ} = \left(\frac{\rho_0 \sigma_0}{2m_\chi m_{T,N}^2} \right) F^2(Q) \int_{v_{\min}}^{v_{\max}} \left[\frac{f_1(v)}{v} \right] dv. \quad (1)$$

*Speaker

Here R is the event rate, i.e., the number of events per unit time and unit mass of detector material, Q is the energy deposited in the detector, ρ_0 is the WIMP density near the Earth, σ_0 is the total cross section ignoring the form factor suppression, $F(Q)$ is the elastic nuclear form factor, $f_1(v)$ is the one-dimensional velocity distribution function of incident WIMPs, v is the absolute value of the WIMP velocity in the laboratory frame. The reduced mass $m_{r,N}$ is defined by $m_{r,N} \equiv m_\chi m_N / (m_\chi + m_N)$, where m_χ is the WIMP mass and m_N that of the target nucleus. Finally, $v_{\min} = \alpha\sqrt{Q}$ with $\alpha \equiv \sqrt{m_N/2m_{r,N}^2}$ is the minimal incoming velocity of incident WIMPs that can deposit the energy Q in the detector, and v_{\max} is related to the escape velocity from our Galaxy at the position of the Solar system.

The total WIMP–nucleus cross section σ_0 in Eq.(1) depends on the nature of the WIMP couplings on nucleons. Generally speaking, one has to distinguish spin-independent (SI) and spin-dependent (SD) couplings. Through e.g., squark and Higgs exchanges with quarks, Majorana WIMPs e.g., neutralinos in the supersymmetric models, can have a SI scalar interaction with nuclei^{1, 2}:

$$\sigma_0^{\text{SI}} = A^2 \left(\frac{m_{r,N}}{m_{r,p}} \right)^2 \sigma_{\chi p}^{\text{SI}}, \quad \sigma_{\chi p}^{\text{SI}} = \left(\frac{4}{\pi} \right) m_{r,p}^2 |f_p|^2, \quad (2)$$

where A is the atomic number of target nucleus, $m_{r,p}$ is the reduced mass of WIMPs and protons, and f_p is the effective $\chi\chi pp$ four-point coupling. Note here that the approximation $f_n \simeq f_p$ predicted in most theoretical models has been adopted and the tiny mass difference between a proton and a neutron has been neglected.

Meanwhile, through e.g., squark and Z boson exchanges with quarks, WIMPs can couple to the spin of the target nuclei. The total cross section for the spin coupling can be expressed as^{1, 2}

$$\sigma_0^{\text{SD}} = \left(\frac{32}{\pi} \right) G_F^2 m_{r,N}^2 \left(\frac{J+1}{J} \right) \left[\langle S_p \rangle a_p + \langle S_n \rangle a_n \right]^2, \quad (3a)$$

and

$$\sigma_{\chi(p,n)}^{\text{SD}} = \left(\frac{24}{\pi} \right) G_F^2 m_{r,p}^2 |a_{(p,n)}|^2. \quad (3b)$$

Here G_F is the Fermi constant, J is the total spin of the target nucleus, $\langle S_{(p,n)} \rangle$ are the expectation values of the proton and the neutron group spins, and $a_{(p,n)}$ is the effective SD WIMP coupling to protons and neutrons.

2. Determining the WIMP mass

It has been found that the one-dimensional velocity distribution function of incident WIMPs, $f_1(v)$, can be solved analytically from Eq.(1) directly⁵ and, consequently, its generalized moments can be estimated by⁶

$$\begin{aligned} & \langle v^n \rangle(v(Q_{\min}), v(Q_{\max})) \\ &= \int_{v(Q_{\min})}^{v(Q_{\max})} v^n f_1(v) dv \\ &= \alpha^n \left[\frac{2Q_{\min}^{(n+1)/2} r(Q_{\min})/F^2(Q_{\min}) + (n+1)I_n(Q_{\min}, Q_{\max})}{2Q_{\min}^{1/2} r(Q_{\min})/F^2(Q_{\min}) + I_0(Q_{\min}, Q_{\max})} \right]. \end{aligned} \quad (4)$$

Here $v(Q) = \alpha\sqrt{Q}$, $Q_{(\min, \max)}$ are the minimal and maximal cut-off energies of the experimental data set, respectively, $r(Q_{\min}) \equiv (dR/dQ)_{Q=Q_{\min}}$ is an estimated value of the scattering spectrum at $Q = Q_{\min}$, and $I_n(Q_{\min}, Q_{\max})$ can be estimated through the sum:

$$I_n(Q_{\min}, Q_{\max}) = \sum_a \frac{Q_a^{(n-1)/2}}{F^2(Q_a)}, \quad (5)$$

where the sum runs over all events in the data set between Q_{\min} and Q_{\max} .

By requiring that the values of a given moment of $f_1(v)$ estimated by Eq.(4) from two detectors with different target nuclei, X and Y , agree, a general expression for determining m_χ appearing in the prefactor α^n on the right-hand side of Eq.(4) has been found as⁷:

$$m_\chi|_{\langle v^n \rangle} = \frac{\sqrt{m_X m_Y} - m_X(\mathcal{R}_{n,X}/\mathcal{R}_{n,Y})}{\mathcal{R}_{n,X}/\mathcal{R}_{n,Y} - \sqrt{m_X/m_Y}}, \quad (6)$$

where

$$\mathcal{R}_{n,X} \equiv \left[\frac{2Q_{\min,X}^{(n+1)/2} r_X(Q_{\min,X})/F_X^2(Q_{\min,X}) + (n+1)I_{n,X}}{2Q_{\min,X}^{1/2} r_X(Q_{\min,X})/F_X^2(Q_{\min,X}) + I_{0,X}} \right]^{1/n}, \quad (7)$$

and $\mathcal{R}_{n,Y}$ can be defined analogously. Here $n \neq 0$, $m_{(X,Y)}$ and $F_{(X,Y)}(Q)$ are the masses and the form factors of the nucleus X and Y , respectively. Note that, since the general moments of $f_1(v)$ estimated by Eq.(4) are independent of the WIMP-nucleus cross section σ_0 , the estimator (6) of m_χ can be used either for SI or for SD scattering.

Additionally, since in most theoretical models the SI WIMP-nucleus cross section given in Eq.(2) dominates^{1, 2}, and on the right-hand side of Eq.(1) is in fact the minus-first moment of $f_1(v)$, which can be estimated

by Eq.(4) with $n = -1$, one can find that⁶

$$\rho_0 |f_p|^2 = \frac{\pi}{4\sqrt{2}} \left(\frac{m_\chi + m_N}{\mathcal{E} A^2 \sqrt{m_N}} \right) \left[\frac{2Q_{\min}^{1/2} r(Q_{\min})}{F^2(Q_{\min})} + I_0 \right]. \quad (8)$$

Here \mathcal{E} is the exposure of the experiment which relates the actual counting rate to the normalized rate in Eq.(1). Since the unknown factor $\rho_0 |f_p|^2$ on the left-hand side above is identical for different targets, it leads to a second expression for determining m_χ ⁶:

$$m_\chi|_\sigma = \frac{(m_X/m_Y)^{5/2} m_Y - m_X(\mathcal{R}_{\sigma,X}/\mathcal{R}_{\sigma,Y})}{\mathcal{R}_{\sigma,X}/\mathcal{R}_{\sigma,Y} - (m_X/m_Y)^{5/2}}. \quad (9)$$

Here $m_{(X,Y)} \propto A_{(X,Y)}$ has been assumed,

$$\mathcal{R}_{\sigma,X} \equiv \frac{1}{\mathcal{E}_X} \left[\frac{2Q_{\min,X}^{1/2} r_X(Q_{\min,X})}{F_X^2(Q_{\min,X})} + I_{0,X} \right], \quad (10)$$

and similarly for $\mathcal{R}_{\sigma,Y}$.

In order to yield the best-fit WIMP mass as well as its statistical error by combining the estimators for different n in Eq.(6) with each other and with the estimator in Eq.(9), a χ^2 function has been introduced⁶

$$\chi^2(m_\chi) = \sum_{i,j} (f_{i,X} - f_{i,Y}) \mathcal{C}_{ij}^{-1} (f_{j,X} - f_{j,Y}), \quad (11)$$

where

$$f_{i,X} \equiv \left(\frac{\alpha_X \mathcal{R}_{i,X}}{300 \text{ km/s}} \right)^i, \quad \text{for } i = -1, 1, 2, \dots, n_{\max}, \quad (12a)$$

and

$$f_{n_{\max}+1,X} \equiv \frac{A_X^2}{\mathcal{R}_{\sigma,X}} \left(\frac{\sqrt{m_X}}{m_\chi + m_X} \right); \quad (12b)$$

the other $n_{\max} + 2$ functions $f_{i,Y}$ can be defined analogously. Here n_{\max} determines the highest moment of $f_1(v)$ that is included in the fit. The f_i are normalized such that they are dimensionless and very roughly of order unity. Note that the first $n_{\max} + 1$ fit functions depend on m_χ through the overall factor α and that m_χ in Eqs.(12a) and (12b) is now a fit parameter, which may differ from the true value of the WIMP mass. Moreover, \mathcal{C} is the total covariance matrix. Since the X and Y quantities are statistically completely independent, \mathcal{C} can be written as a sum of two terms:

$$\mathcal{C}_{ij} = \text{cov}(f_{i,X}, f_{j,X}) + \text{cov}(f_{i,Y}, f_{j,Y}). \quad (13)$$

Finally, since we require that, from two experiments with different target nuclei, the values of a given moment of the WIMP velocity distribution estimated by Eq.(4) should agree, this means that the upper cuts on $f_1(v)$ in two data sets should be (approximately) equal[†]. This requires that⁶

$$Q_{\max,Y} = \left(\frac{\alpha_X}{\alpha_Y} \right)^2 Q_{\max,X}. \quad (14)$$

Note that α is a function of the true WIMP mass. Thus this relation for matching optimal cut-off energies can be used only if m_χ is already known. One possibility to overcome this problem is to fix the cut-off energy of the experiment with the heavier target, minimize the $\chi^2(m_\chi)$ function defined in Eq.(11), and estimate the cut-off energy for the lighter nucleus by Eq.(14) algorithmically⁶.

As demonstration we show some numerical results for the reconstructed WIMP mass based on Monte Carlo simulations. The upper and lower bounds on the reconstructed WIMP mass are estimated from the requirement that χ^2 exceeds its minimum by 1. ^{28}Si and ^{76}Ge have been chosen as two target nuclei. The scattering cross section has been assumed to be dominated by spin-independent interactions. The theoretically predicted recoil spectrum for the shifted Maxwellian velocity distribution ($v_0 = 220$ km/s, $v_e = 231$ km/s)^{1, 2, 5} with the Woods-Saxon elastic form factor^{8, 1, 2} have been used. The threshold energies of two experiments have been assumed to be negligible and the maximal cut-off energies are set as 100 keV. $2 \times 5,000$ experiments with 50 events on average before cuts from each experiment have been simulated. In order to avoid large contributions from very few events in the high energy range to the higher moments⁵, only the moments up to $n_{\max} = 2$ have been included in the χ^2 fit.

In Fig. 1 the dotted (green) curves show the median reconstructed WIMP mass and its 1σ upper and lower bounds for the case that both Q_{\max} have been fixed to 100 keV. This causes a systematic *underestimate* of the reconstructed WIMP mass for input WIMP masses $\gtrsim 100$ GeV⁷. The solid (black) curves have been obtained by using Eq.(14) for matching the cut-off energy $Q_{\max,\text{Si}}$ perfectly with $Q_{\max,\text{Ge}} = 100$ keV and the true (input) WIMP mass, whereas the dashed (red) curves show the case that $Q_{\max,\text{Ge}} = 100$ keV, and $Q_{\max,\text{Si}}$ has been determined by minimizing $\chi^2(m_\chi)$. As shown here, with only 50 events from one experiment, the algorithmic process seems already to work pretty well for WIMP masses

[†]Here the threshold energies have been assumed to be negligibly small.

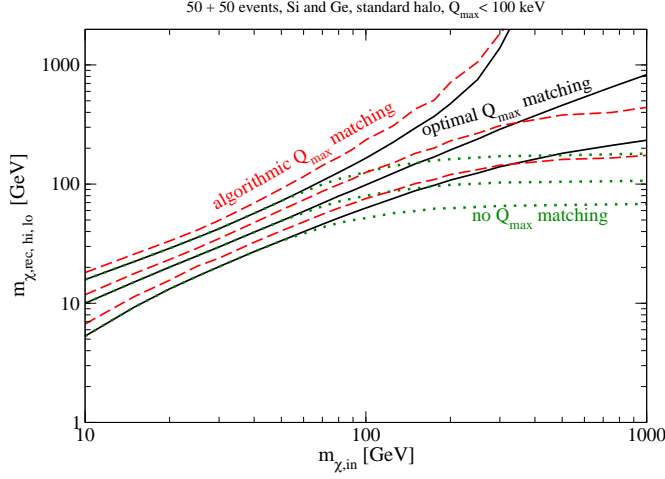


Fig. 1. Results for the median reconstructed WIMP mass as well as its 1σ statistical error interval based on the χ^2 -fit in Eq.(11). See the text for further details.

up to ~ 500 GeV. Though for $m_\chi \lesssim 100$ GeV m_χ determined in this way *overestimates* its true value by 15 to 20%, the true WIMP mass always lies within the median limits of the 1σ statistical error interval up to even $m_\chi = 1$ TeV⁶.

On the other hand, in order to study the statistical fluctuation of the reconstructed WIMP mass by algorithmic Q_{\max} matching in the simulated experiments, an estimator δm has been introduced as⁶

$$\delta m = \begin{cases} 1 + \frac{m_{\chi,lo1} - m_{\chi,in}}{m_{\chi,lo1} - m_{\chi,lo2}}, & \text{if } m_{\chi,in} \leq m_{\chi,lo1}; \\ \frac{m_{\chi,rec} - m_{\chi,in}}{m_{\chi,rec} - m_{\chi,lo1}}, & \text{if } m_{\chi,lo1} < m_{\chi,in} < m_{\chi,rec}; \\ \frac{m_{\chi,rec} - m_{\chi,in}}{m_{\chi,hi1} - m_{\chi,rec}}, & \text{if } m_{\chi,rec} < m_{\chi,in} < m_{\chi,hi1}; \\ \frac{m_{\chi,hi1} - m_{\chi,in}}{m_{\chi,hi2} - m_{\chi,hi1}} - 1, & \text{if } m_{\chi,in} \geq m_{\chi,hi1}. \end{cases} \quad (15)$$

Here $m_{\chi,in}$ is the true (input) WIMP mass, $m_{\chi,rec}$ its reconstructed value, $m_{\chi,lo1(2)}$ are the 1 (2) σ lower bounds satisfying $\chi^2(m_{\chi,lo(1,2)}) = \chi^2(m_{\chi,rec}) + 1$ (4), and $m_{\chi,hi1(2)}$ are the corresponding 1 (2) σ upper bounds.

Figures 2 show the distribution of the estimator δm calculated from 5,000 simulated experiments for WIMP masses of 50 GeV (left) and 200

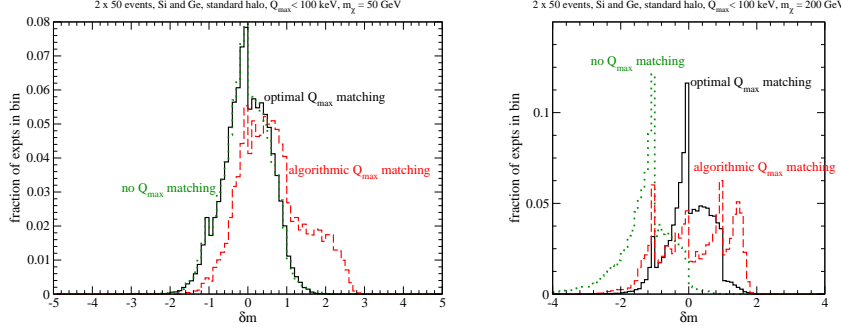


Fig. 2. Normalized distribution of the estimator δm defined in Eq.(15) for WIMP masses of 50 GeV (left) and 200 GeV (right). Parameters and notations are as in Fig. 1. Here the bins at $\delta m = \pm 5$ are overflow bins, i.e., they also contain all experiments with $|\delta m| \geq 5$.

GeV (right). For the lighter WIMP mass, simply fixing both Q_{\max} values to 100 keV still works fine (the dotted (green) curves in Fig. 1). However, the distributions for both fixed Q_{\max} and optimal Q_{\max} matching show already an asymmetry of the statistical uncertainties with $m_{\chi, \text{hi1}} - m_{\chi, \text{rec}} > m_{\chi, \text{rec}} - m_{\chi, \text{lo1}}$. The overestimate of light WIMP masses reconstructed by algorithmic Q_{\max} matching shown in Fig. 1 is also reflected by the dashed (red) histogram here, which has significantly more entries at positive values than at negative values. Moreover, these distributions also indicate that the statistical uncertainties estimated by minimizing $\chi^2(m_\chi)$ are in fact overestimated, since nearly 90% of the simulated experiments have $|\delta m| \leq 1^6$, much more than $\sim 68\%$ of the experiments, which a usual 1σ error interval should contain.

For the heavier WIMP mass of 200 GeV, as shown in the right frame of Figs. 2, the situation becomes less favorable. While the distributions for both fixed Q_{\max} and optimal Q_{\max} matching look more non-Gaussian but more concentrated on the median values, the distribution for algorithmic Q_{\max} matching spreads out in the range $-1 < \delta m < 2$. It has even been observed that, for larger samples (e.g., with 500 events on average) the outspread distribution becomes broader⁶. Hence, the statistical fluctuation by the algorithmic procedure for determining Q_{\max} of the experiment with the lighter target nucleus by minimizing χ^2 could be problematic for the determination of m_χ if WIMPs are heavy.

3. Estimating the SI WIMP–proton coupling

As shown in the previous section, by combining two experimental data sets, one can estimate the WIMP mass m_χ without knowing the WIMP–nucleus cross section σ_0 . Conversely, by using Eq.(8), one can also estimate the SI WIMP–proton coupling, $|f_p|^2$, from experimental data directly *without* knowing the WIMP mass⁹.

In Eq.(8) the WIMP mass m_χ on the right–hand side can be determined by the method described in Sec. 2, $r(Q_{\min})$ and I_0 can also be estimated from one of the two data sets used for determining m_χ or from a third experiment. However, due to the degeneracy between the local WIMP density ρ_0 and the coupling $|f_p|^2$, one *cannot* estimate each one of them without making some assumptions. The simplest way is making an assumption for the local WIMP density ρ_0 .

Figure 3 shows the reconstructed SI WIMP–proton coupling as a function of the input WIMP mass.. The WIMP mass has again been reconstructed with ^{28}Si and ^{76}Ge . In order to avoid complicated calculations of the correlation between the error on the reconstructed m_χ and that on the estimator of I_0 , a second, independent data set with Ge has been chosen as the third target for estimating I_0 . Parameters are as in Fig. 1, except that the SI WIMP–proton cross section has been set as 10^{-8} pb.

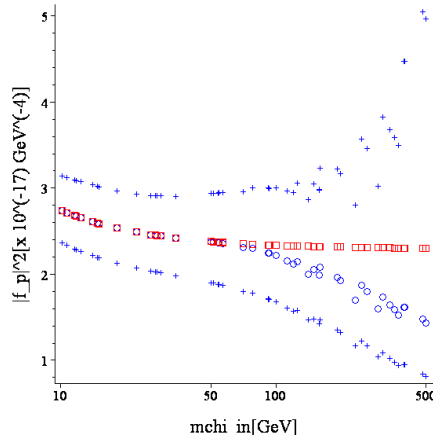


Fig. 3. The reconstructed SI WIMP–proton coupling as a function of the input WIMP mass. The (red) squares indicate the input WIMP masses and the true values of the coupling. The (blue) circles and the (blue) crosses indicate the reconstructed couplings and their 1σ statistical errors. Parameters are as in Fig. 1, in addition $\sigma_{\chi p}^{\text{SI}}$ has been set as 10^{-8} pb. See the text for further details.

It can be seen that the reconstructed $|f_p|^2$ are *underestimated* for WIMP masses $\gtrsim 100$ GeV. This systematic deviation is caused mainly by the underestimate of I_0 . However, in spite of this systematic deviation the true value of $|f_p|^2$ always lies within the 1σ statistical error interval. Moreover, for a WIMP mass of 100 GeV, one could in principle already estimate the SI WIMP–proton coupling with a statistical uncertainty of only $\sim 15\%$ with just 50 events from each experiment. Note that this is much smaller than the systematic uncertainty of the local Dark Matter density (of a factor of 2 or even larger).

4. Determining ratios of WIMP–nucleon cross sections

So far we have discussed only the case that the spin-independent WIMP–nucleus interaction dominates. In this section we turn to consider the case of the spin-dependent cross section as well as of a general combination of these two cross sections.

4.1. Determining the a_n/a_p ratio

Consider at first the case that the SD WIMP–nucleus interaction dominates. By substituting σ_0^{SD} in Eq.(3a) and $\langle v^{-1} \rangle$ estimated by Eq.(4) into Eq.(1) and combining two data sets with different target nuclei, an expression for the ratio between two SD WIMP–nucleon couplings can be given as

$$\left(\frac{a_n}{a_p}\right)_{\pm,n}^{\text{SD}} = -\frac{\langle S_p \rangle_X \mathcal{R}_{J,n,Y} \pm \langle S_p \rangle_Y \mathcal{R}_{J,n,X}}{\langle S_n \rangle_X \mathcal{R}_{J,n,Y} \pm \langle S_n \rangle_Y \mathcal{R}_{J,n,X}}, \quad (16)$$

with

$$\mathcal{R}_{J,n,X} \equiv \left[\left(\frac{J_X}{J_X + 1} \right) \frac{\mathcal{R}_{\sigma,X}}{\mathcal{R}_{n,X}} \right]^{1/2}, \quad (17)$$

and similarly for $\mathcal{R}_{J,n,Y}$, where $n \neq 0$. Note that a_n/a_p can be estimated from experimental data directly through estimating $\mathcal{R}_{n,X}$, $\mathcal{R}_{\sigma,X}$ and two Y terms by Eqs.(7) and (10)[‡] *without* knowing the WIMP mass.

Because the couplings in Eq.(3a) are squared, we have two solutions for a_n/a_p here; if exact “theory” values for $\mathcal{R}_{J,n,(X,Y)}$ are taken, these solutions coincide for $a_n/a_p = -\langle S_p \rangle_X / \langle S_n \rangle_X$ and $-\langle S_p \rangle_Y / \langle S_n \rangle_Y$, which depends only on the properties of target nuclei[§]. Moreover, one of these

[‡]Note that the form factor $F^2(Q)$ here must be chosen for the SD cross section.

[§]Some relevant spin values of the nuclei used for our simulations shown in this paper are given in Table. 1.

Table 1. List of the relevant spin values of the nuclei used for simulations shown in this paper (Data from Ref. 10).

nucleus	Z	J	$\langle S_p \rangle$	$\langle S_n \rangle$	$-\langle S_p \rangle / \langle S_n \rangle$
^{17}O	8	5/2	0	0.495	0
^{23}Na	11	3/2	0.248	0.020	-12.40
^{37}Cl	17	3/2	-0.058	0.050	1.16
^{73}Ge	32	9/2	0.030	0.378	-0.079

two solutions has a pole at the middle of two intersections, which depends simply on the signs of $\langle S_n \rangle_X$ and $\langle S_n \rangle_Y$: since $\mathcal{R}_{J,n,X}$ and $\mathcal{R}_{J,n,Y}$ are always positive, if both of $\langle S_n \rangle_X$ and $\langle S_n \rangle_Y$ are positive or negative, the “minus” solution $(a_n/a_p)_{-,n}^{\text{SD}}$ will diverge and the “plus” solution $(a_n/a_p)_{+,n}^{\text{SD}}$ will be the “inside” solution, which has a smaller statistical uncertainty (see Figs. 4); in contrast, if the signs of $\langle S_n \rangle_X$ and $\langle S_n \rangle_Y$ are opposite, the “minus” solution $(a_n/a_p)_{-,n}^{\text{SD}}$ will be the “inside” solution.

Figures 4 show the reconstructed $(a_n/a_p)^{\text{SD}}$ estimated by Eq.(16) with $n = 1$ as functions of the true (input) a_n/a_p for a WIMP mass of 100 GeV (left) and as functions of the input WIMP masses for $a_n/a_p = 0.7$ (right), respectively. The shifted Maxwellian velocity distribution with a form factor calculated in the thin-shell approximation for the SD cross section^{4, 11} has been used. Parameters are as earlier, except that the minimal cut-off energy has been increased to 5 keV for both experiments. Here we have

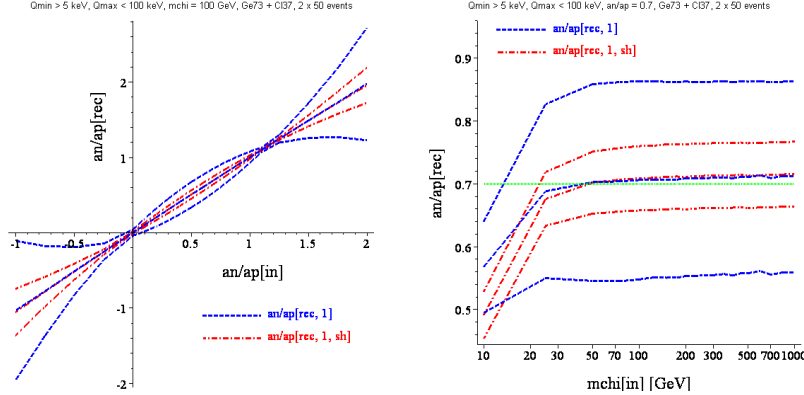


Fig. 4. Preliminary results for the reconstructed $(a_n/a_p)^{\text{SD}}$ estimated by Eq.(16) with $n = 1$ as functions of the true (input) a_n/a_p (left frame, for a WIMP mass of 100 GeV) and as functions of the input WIMP mass m_χ (right frame, for $a_n/a_p = 0.7$), respectively. See the text for further details.

chosen ^{73}Ge and ^{37}Cl as two target nuclei in order to test the range of interest $0 \leq a_n/a_p \leq 1^{12, 13}$; and $(a_n/a_p)_{+/-,n}^{\text{SD}}$ are thus the inside/outside solutions.

For estimating the statistical error on a_n/a_p , one needs to estimate the counting rate at the threshold energy, $r(Q_{\min})$, and its statistical error, $\sigma(r(Q_{\min}))$. It has been found that, instead of Q_{\min} , one can estimate the counting rate and its statistical error at the shifted point $Q_{s,1}$ (from the central point of the first bin, Q_1)⁵:

$$Q_{s,1} = Q_1 + \frac{1}{k_1} \ln \left[\frac{\sinh(k_1 b_1/2)}{k_1 b_1/2} \right], \quad (18)$$

where k_1 is the logarithmic slope of the reconstructed recoil spectrum in the first Q -bin and b_1 is the bin width. We see in the right frame of Figs. 4 very clearly that, for WIMP masses $\gtrsim 30$ GeV, the 1σ statistical error estimated with $Q_{s,1}$ (the dash-dotted (red) lines, labeled with “sh”) is $\sim 7\%$, only 1/3 of the error estimated with Q_{\min} (the dashed (blue) lines).

One more advantage with using $Q_{s,1}$ instead of Q_{\min} is that the statistical error on a_n/a_p estimated with different n (namely with different moments of the WIMP velocity distribution) at $Q = Q_{s,1}$ are almost equal. Therefore, since

$$\mathcal{R}_{J,-1,X} = \left[\left(\frac{J_X}{J_X + 1} \right) \frac{2 r_X(Q_{X,s,1})}{\mathcal{E}_X F_X^2(Q_{X,s,1})} \right]^{1/2}, \quad (19)$$

one needs thus only events in the low energy range (~ 20 events between 5 and 15 keV in our simulations) for estimating a_n/a_p .

4.2. Determining the $\sigma_{\chi\text{p}/\text{n}}^{\text{SD}}/\sigma_{\chi\text{p}}^{\text{SI}}$ ratios

Now let us combine WIMP-nucleus scattering induced by both SI and SD interactions given in Eqs.(2) and (3a) (with the corresponding form factors). By modifying $F^2(Q)$ and I_n in the estimator (4) of the moments of the WIMP velocity distribution, the ratio of the SD WIMP-proton cross section to the SI one can be solved analytically as^{¶, ||}

$$\frac{\sigma_{\chi\text{p}}^{\text{SD}}}{\sigma_{\chi\text{p}}^{\text{SI}}} = - \frac{F_{\text{SI},X}^2(Q_{\min,X})\mathcal{R}_{m,Y} - F_{\text{SI},Y}^2(Q_{\min,Y})\mathcal{R}_{m,X}}{\mathcal{C}_{\text{p},X}F_{\text{SD},X}^2(Q_{\min,X})\mathcal{R}_{m,Y} - \mathcal{C}_{\text{p},Y}F_{\text{SD},Y}^2(Q_{\min,Y})\mathcal{R}_{m,X}}. \quad (20)$$

[¶]In this section we consider only the case of $\sigma_{\chi\text{p}}^{\text{SD}}$, but all formulae given here can be applied straightforwardly to the case of $\sigma_{\chi\text{n}}^{\text{SD}}$ by exchanging $\text{n} \leftrightarrow \text{p}$.

^{||} Q_{\min} appearing in this section can be replaced by $Q_{s,1}$ everywhere.

12

Here

$$\mathcal{R}_{m,X} \equiv \frac{r_X(Q_{\min,X})}{\mathcal{E}_X m_X^2}, \quad (21)$$

and

$$\mathcal{C}_{p,X} \equiv \frac{4}{3} \left(\frac{J_X + 1}{J_X} \right) \left[\frac{\langle S_p \rangle_X + \langle S_n \rangle_X (a_n/a_p)}{A_X} \right]^2; \quad (22)$$

$\mathcal{R}_{m,Y}$ and $\mathcal{C}_{p,Y}$ can be defined analogously. Note that a “minus (−)” sign appears in the expression (20).

By introducing a third target having *only* the SI interaction with WIMPs, a_n/a_p appearing in $\mathcal{C}_{p,X}$ and $\mathcal{C}_{p,Y}$ can again be solved analytically as

$$\left(\frac{a_n}{a_p} \right)_{\pm}^{\text{SI+SD}} = \frac{-(c_{p,X} s_{n/p,X} - c_{p,Y} s_{n/p,Y}) \pm \sqrt{c_{p,X} c_{p,Y}} |s_{n/p,X} - s_{n/p,Y}|}{c_{p,X} s_{n/p,X}^2 - c_{p,Y} s_{n/p,Y}^2}. \quad (23)$$

Here

$$c_{p,X} \equiv \frac{4}{3} \left(\frac{J_X + 1}{J_X} \right) \left(\frac{\langle S_p \rangle_X}{A_X} \right)^2 F_{\text{SD},X}^2(Q_{\min,X}) \\ \times \left[F_{\text{SI},Z}^2(Q_{\min,Z}) \left(\frac{\mathcal{R}_{m,Y}}{\mathcal{R}_{m,Z}} \right) - F_{\text{SI},Y}^2(Q_{\min,Y}) \right], \quad (24)$$

$c_{p,Y}$ can be obtained by simply exchanging $X \leftrightarrow Y$, and $s_{n/p} \equiv \langle S_n \rangle / \langle S_p \rangle$. However, in order to reduce the statistical uncertainties contributed from estimate of a_n/a_p involved in $\mathcal{C}_{p,X}$ and $\mathcal{C}_{p,Y}$, one can use one target with the SD sensitivity (almost) only to protons or to neutrons combined with another one with only the SI sensitivity. For this case $\mathcal{C}_{p,X}$ is independent of a_n/a_p and the expression (20) for $\sigma_{\chi p}^{\text{SD}}/\sigma_{\chi p}^{\text{SI}}$ can be reduced to

$$\frac{\sigma_{\chi p}^{\text{SD}}}{\sigma_{\chi p}^{\text{SI}}} = - \frac{F_{\text{SI},X}^2(Q_{\text{thre},X}) \mathcal{R}_{m,Y} - F_{\text{SI},Y}^2(Q_{\text{thre},Y}) \mathcal{R}_{m,X}}{\mathcal{C}_{p,X} F_{\text{SD},X}^2(Q_{\text{thre},X}) \mathcal{R}_{m,Y}}. \quad (25)$$

Figures 5 show the reconstructed $\sigma_{\chi p}^{\text{SD}}/\sigma_{\chi p}^{\text{SI}}$ (left) and $\sigma_{\chi n}^{\text{SD}}/\sigma_{\chi p}^{\text{SI}}$ (right) estimated by Eqs.(20) and (25) as functions of the true (input) a_n/a_p , respectively. Besides ^{73}Ge and ^{37}Cl , ^{28}Si has been chosen as the third target for estimating a_n/a_p by Eq.(23); whereas ^{76}Ge has been chosen as the second target having only the SI interaction with WIMPs and combined with ^{23}Na (for $\sigma_{\chi p}^{\text{SD}}/\sigma_{\chi p}^{\text{SI}}$) and ^{17}O (for $\sigma_{\chi n}^{\text{SD}}/\sigma_{\chi p}^{\text{SI}}$) for using Eq.(25). We see here that, since the SD WIMP–nucleus interaction doesn’t dominate for our simulation setup, $\sigma_{\chi p}^{\text{SD}}/\sigma_{\chi p}^{\text{SI}}$ estimated by Eq.(20) has two discontinuities around the intersections at $a_n/a_p = -0.079$ and especially at $a_n/a_p = 1.16$,

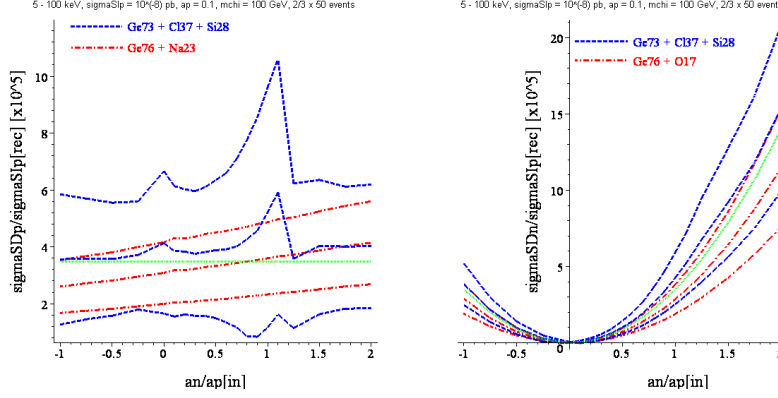


Fig. 5. Preliminary results for the reconstructed $\sigma_{\chi p}^{\text{SD}}/\sigma_{\chi p}^{\text{SI}}$ (left) and $\sigma_{\chi n}^{\text{SD}}/\sigma_{\chi p}^{\text{SI}}$ (right) as functions of the true (input) a_n/a_p , respectively. The dashed (blue) curves indicate the values estimated by Eq.(20) with a_n/a_p estimated by Eq.(23); whereas the dash-dotted (red) curves indicate the values estimated by Eqs.(25). $\sigma_{\chi p}^{\text{SI}}$ and a_p have been set as 10^{-8} pb and 0.1, respectively. The other parameters are as in Figs. 4. Note that, since we fix $\sigma_{\chi p}^{\text{SI}}$ and a_p , $\sigma_{\chi p}^{\text{SD}}/\sigma_{\chi p}^{\text{SI}}$ shown here is a constant, whereas $\sigma_{\chi n}^{\text{SD}}/\sigma_{\chi p}^{\text{SI}} \propto a_n^2$ a parabola.

the intersection determined by the $-\langle S_p \rangle / \langle S_n \rangle$ value of ^{37}Cl . However, from two experiments with only ~ 20 events in the low energy range, one could in principle already estimate $\sigma_{\chi p}^{\text{SD}}/\sigma_{\chi p}^{\text{SI}}$ and $\sigma_{\chi n}^{\text{SD}}/\sigma_{\chi p}^{\text{SI}}$ by using Eq.(25) with a statistical uncertainties of $\sim 35\%$.

5. Summary and conclusions

In this article we described model-independent methods for determining the WIMP mass and their couplings on nucleons by using future experimental data from direct Dark Matter detection. The main focus is *how well* we could extract the nature of WIMPs with *positive* signals and *which problems* we could meet by applying these methods to (real) data analysis.

In Secs. 2 and 3 we discussed the determinations of the WIMP mass and its spin-independent coupling on protons. If WIMPs are light ($m_\chi \simeq 50$ GeV), with $\mathcal{O}(50)$ events from one experiment, their mass and SI coupling could be estimated with errors of $\sim 35\%$ and $\sim 15\%$, respectively. However, in case WIMPs are heavy ($m_\chi \gtrsim 200$ GeV), the statistical fluctuation by the algorithmic procedure for matching the maximal cut-off energies of the experiments could be problematic for estimating their mass, and thereby their SI coupling.

In Sec. 4 we turned to consider the spin-dependent interaction. The simulations show pretty small statistical uncertainties. Moreover, differ-

ing from the traditional method for constraining the SD WIMP–nucleon couplings^{14, 15, 10, 16}, we do not make any assumptions on ρ_0 , $f_1(v)$, and m_χ . The price one has to pay for this is that positive signals in at least two different data sets with different target nuclei are required. In addition, without independent knowledge of ρ_0 , one can only determine ratios of cross sections.

In summary, once two (or more) experiments measure WIMP events, the methods presented here could in principle help us to extract the nature of halo WIMPs. This information will allow us not only to constrain the parameter space in different extensions of the Standard Model, but also to confirm or exclude some candidates for WIMP Dark Matter^{17, 18}.

Acknowledgments

This work was partially supported by the Marie Curie Training Research Network “UniverseNet” under contract no. MRTN-CT-2006-035863, by the European Network of Theoretical Astroparticle Physics ENTApP IL-IAS/N6 under contract no. RII3-CT-2004-506222, as well as by the BK21 Frontier Physics Research Division under project no. BA06A1102 of Korea Research Foundation.

References

1. G. Jungman, M. Kamionkowski, and K. Griest, *Phys. Rep.* **267**, 195 (1996).
2. G. Bertone, D. Hooper, and J. Silk, *Phys. Rep.* **405**, 279 (2005).
3. P. F. Smith and J. D. Lewin, *Phys. Rep.* **187**, 203 (1990).
4. J. D. Lewin and P. F. Smith, *Astropart. Phys.* **6**, 87 (1996).
5. M. Drees and C. L. Shan, *J. Cosmol. Astropart. Phys.* **0706**, 011 (2007).
6. M. Drees and C. L. Shan, *J. Cosmol. Astropart. Phys.* **0806**, 012 (2008).
7. C. L. Shan and M. Drees, [arXiv:0710.4296 \[hep-ph\]](#) (2007).
8. J. Engel, *Phys. Lett. B* **264**, 114 (1991).
9. M. Drees and C. L. Shan, [arXiv:0809.2441 \[hep-ph\]](#) (2008).
10. F. Giuliani and T. A. Girard, *Phys. Rev. D* **71**, 123503 (2005).
11. H. V. Klapdor-Kleingrothaus, I. V. Krivosheina, and C. Tomei, *Phys. Lett. B* **609**, 226 (2005).
12. V. A. Bednyakov, *Phys. Atom. Nucl.* **67**, 1931 (2004).
13. J. Ellis, K. A. Olive, and C. Savage, *Phys. Rev. D* **77**, 065026 (2008).
14. D. R. Tovey *et al.*, *Phys. Lett. B* **488**, 17 (2000).
15. F. Giuliani, *Phys. Rev. Lett.* **93**, 161301 (2004).
16. T. A. Girard and F. Giuliani, *Phys. Rev. D* **75**, 043512 (2007).
17. G. Bertone *et al.*, *Phys. Rev. Lett.* **99**, 151301 (2007).
18. V. Barger, W. Y. Keung, and G. Shaughnessy, *Phys. Rev. D* **78**, 056007 (2008).